JMEPEG (2012) 21:153–160
DOI: 10.1007/s11665-011-9928-x

1059-9495/$19.00

Buckling Distortions and Mitigation Techniques for Thin-Section Structures

Y.P. Yang and P. Dong

(Submitted August 7, 2010; in revised form February 3, 2011)

The underlying mechanisms associated with welding-induced buckling distortions are investigated using finite element procedures. Unlike stable type of welding-induced distortions which can be adequately captured by performing a thermo-plasticity simulation of actual welding procedures, local buckling distortions in welded structures are of an unstable type, which requires the use of appropriate buckling analysis procedures incorporating welding-induced residual stress state. With the underlying mechanisms in buckling distortions being established, two effective mitigation techniques were presented. One is trailing heat sink and the other is in-process synchronized rolling techniques. Detailed finite element simulations were performed to demonstrate how some of the important process parameters can be established in effectively reducing or eliminating the buckling distortions. The proposed techniques were also validated by laboratory welding trials. The underlying principles and potential applications of the distortion mitigation techniques are also discussed in light of the detailed finite element simulation results.

Keywords buckling distortion, finite element method, in-process rolling, trailing heat sink, welded structures, welding process modeling

1. Introduction

Thin-gauge materials are increasingly used in today's high-performance welded-structures in automotive, aircraft, ship-building, and other industries. It is well known that buckling distortions have been a major concern in welding fabrication of such structures. Both past research efforts such as those by Masubuchi (Ref 1) and recent investigations (Ref 2-8) in this area have established that compressive residual stresses contribute to the development of a specific buckling mode in a given component. There is a growing interest in developing effective finite element procedures for predicting buckling distortions (Ref 6-12), particularly in terms of relating a particular residual stress distribution to a specific buckling mode. Only then, can the effects of welding procedures and additional in-process mitigation techniques (Ref 9-18) be quantitatively evaluated for their effectiveness in producing a favorable residual stress state that minimizes the likelihood of setting off a particular buckling mode during and after welding fabrication.

To understand the buckling mechanism and assist the development of buckling controlling techniques, finite element-based analysis techniques were developed (Ref 9-18). Michaleris and Sun (Ref 9) used 2D approximation to the longitudinal (along weld direction) residual stress state in a 3D T-fillet joint. Then, elastic buckling modal analysis was performed using an equivalent thermal load to the 2D model. The method is attractive in its simplicity and was demonstrated effective for the cases reported (Ref 9). However, one limitation of this analysis procedure is that residual stress distribution and weld sequence effects on buckling distortion cannot be assessed, since the complex history effects on residual stress and deformation developments in such situations cannot be captured in both stages of the analysis procedure proposed. Deo et al. (Ref 8, 10) used a rather similar buckling analysis method, except that a residual stress value away from weld in the 2D residual stress field was used to correlate with critical buckling loads with respect to elastic buckling modal analysis under a unit thermal load condition.

Earlier efforts in mitigating welding-induced buckling distortions are primarily experimental in nature. For instance, Masubuchi (Ref 1) discussed the effects of pre-straining using either mechanical or thermal means. Guan et al. (Ref 14) presented an effective in-process buckling distortion mitigation technique that employs an in-process trailing heat sink technique which provides stretching effects on weld metal on cooling. A subsequent analysis by Yang et al. (Ref 6) and Van et al. (Ref 11) using a finite element method incorporating residual stress distribution demonstrated that both compressive residual stress magnitude and the overall full-field distribution characteristics contributed to the effectiveness of this method. With this understanding, this technique has been used to control buckling distortion in titanium thin sheet (Ref 12). Recently, this technique had been used to control distortion during friction stir welding (Ref 13).

A thermal tensioning technique for controlling welding residual stress and distortion was first investigated by Bural et al. (Ref 15), involving imparting tensile stress at the weld zone, prior to and during welding by imposing a preset

Y.P. Yang, Edison Welding Institute, 1250 Arthur E. Adams Drive, Columbus, OH; and **P. Dong**, The University of New Orleans, 2000 Lakeshore Drive, New Orleans, LA 70148. Contact e-mail: yyang@ewi.org.

steady-state temperature gradient. This technique was recently investigated further by Michaleris et al. (Ref 9), Deo et al. (Ref 10), and Yang et al. (Ref 7) both experimentally and numerically, on its effectiveness of a stationary side-by-side heating/cooling combination on a stiffened panel weldment.

Since some materials such as high strength steels are sensitive to heating and cooling, the trailing heat sink technique and the transient thermal tensioning technique may not be applicable to control buckling distortion and weld residual stress. Mechanical rolling technique was investigated for this purpose (Ref 16, 17). Altenkirch et al. (Ref 17) placed two rollers at both sides of weld during FSW. Although this two-roller setup successfully controlled hot cracking (Ref 16), it produced minimum effect in controlling residual stress and distortion (Ref 17). Post-welding rolling was also conducted by applying a single roller directly on the FSW weld line. In this case, significant effects were observed with increased loading, causing a marked reduction in the longitudinal tensile residual stress (Ref 17). The disadvantage of mechanical rolling technique is that special tooling design has to be done for applying this technique. Therefore, noncontact electromagnetic impact technique was proposed and demonstrated its effectiveness in controlling buckling distortion (Ref 18). All the techniques mentioned above follow essentially the same principle that local buckling tendency can be minimized by reducing or altering a compressive residual stress distribution that otherwise would promote a particular buckling mode.

In this article, the underlying mechanics associated with buckling distortion are first presented, particularly by contrasting with typical stable type of distortions. An effective finite element procedure for predicting buckling distortions is then presented, in which a given full-field residual stress state can be directly related to the most likely buckling mode for a given welded component. With such analysis procedures, various mitigation techniques for modifying residual stress distributions and their effects on reducing or eliminating buckling distortions are evaluated. Both a trailing heat sink technique and a new in-process synchronized rolling technique are found to be particularly effective. With their proper parameters being qualitatively established in a series of finite element simulation, experimental welding trials have been conducted to validate their effectiveness. The in-process synchronized rolling technique is novel and possesses various additional advantages such as significantly improved weld performance in service.

2. Buckling Distortion Mechanisms

2.1 Analytical-Based Buckling Distortion Analysis

Buckling distortions due to welding-induced residual stresses can be simply illustrated by considering a plate subjected to a given longitudinal residuals stress field ($\sigma_x(y)$) in Fig. 1(a). For simplicity, only one weld is considered in the middle of the plate, as shown in Fig. 1(a). Resorting to classical elastic structural mechanics theory (Ref 19), one can obtain the following governing equations with respect to out-of-plane displacement w:

$$\frac{\partial^4 w}{\partial x^4} + 2\frac{\partial^4 w}{\partial x^2 \partial y^2} + \frac{\partial^4 w}{\partial y^4} = \frac{N_x}{D}\left(\frac{\partial^2 w}{\partial x^2}\right) \qquad \text{(Eq 1)}$$

where

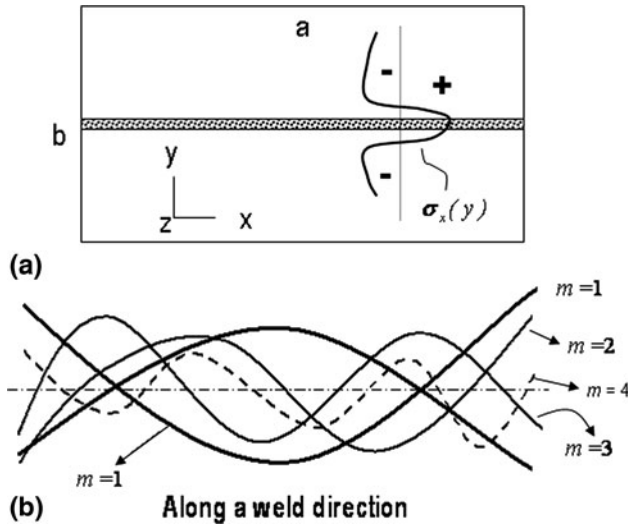

Fig. 1 Illustration of weld residual stress-induced buckling. (a) Buckling problem definition for a plate with an aspect ratio of a/b, (b) illustration of buckling instabilities with various wave lengths

$$D = \frac{Et^3}{12(1-\nu^2)}$$

$$N_x = \lambda \cdot \int_{-t/2}^{t/2} \sigma_x(y,z)\,dz$$

Equation 1 ignores the end effects in the longitudinal welds, so the in-plane unit force N_x depends only on the y-coordinate after the through-thickness integration. Note that N_x, as a measure of a distributed line force contributed by the longitudinal residual stress component in Fig. 1(a). The scaling parameter λ for a given residual stress distribution is introduced here for convenience in constructing numerical solutions in performing buckling mode identification in the next section. D is the flexural modulus as a function of Young's modulus E, Poisson ratio ν, and plate thickness t. Equation 1 can be easily solved if the line force N_x is assumed to be invariant in y, which can be viewed a reasonable assumption if the local buckling wave length is relatively small in the width direction. The solution of the buckling problem as stated in Fig. 1(a) becomes, under simply supported conditions:

$$w = \sum_{m=1}^{\infty}\sum_{n=1}^{\infty} a_{mn} \sin\frac{m\pi x}{a}\sin\frac{n\pi y}{b} \qquad \text{(Eq 2)}$$

Then, the corresponding residual stress levels when buckling develops can be calculated as:

$$N_x = \frac{\pi^2 a^2 D}{m^2}\left(\frac{m^2}{a^2} + \frac{n^2}{b^2}\right)^2 \qquad \text{(Eq 3)}$$

Without losing generality, one can set $n = m = 1$ (i.e., one-half buckling wave with respect to x and y) to obtain the minimum critical compressive line force due to weld residual stresses:

$$(N_x)_{cr} = \frac{\pi^2 D}{b^2}\left(\frac{b}{a} + \frac{a}{b}\right)^2 = k\frac{\pi^2 D}{b^2} \qquad \text{(Eq 4)}$$

Although various assumptions were introduced in obtaining the closed-form solutions in Eq 3 and 4, the implications are

significant in understanding distortion behaviors as observed in the test panels discussed earlier. For a given plate width (b), the line force (due to compressive residual stresses) is at the minimum when the plate aspect ratio $a/b = 1$. If multiple-half waves in the length direction are considered (i.e., $m = 1, 2, 3, \ldots$, in Eq 3, as illustrated in Fig. 1b), it can be shown that the critical compressive line force in Eq 4 remains the same for $a/b = 1,2, 3, \ldots$. As the plate becomes very long or a/b becomes large, the local buckling half-wave length approaches the width of the plate (b) in Fig. 1(a). Among other things, Eq 4 clearly suggests that in welding assembly of thin plate structures such as those in shipbuilding, a plate aspect ratio (a/b) that maximize the buckling strength should be considered, if practical.

In all cases discussed above, the critical compressive residual stresses on the sides of the weld can be approximately estimated as:

$$\sigma_{cr}^{r} = \frac{k\pi^2 E}{12(1-\nu^2)}\frac{t^2}{b^2} \qquad \text{(Eq 5)}$$

Equation 5 clearly indicates that the buckling resistance decreases drastically in the form of $(t/b)^2$, as the plate thickness t decreases. For instance, if the plate thickness decreases from $t = 10$ mm to 5 mm (current panel thickness), the magnitude of the compressive residual stresses required to trigger buckling is reduced by 75%. In the meantime, the longitudinal residual stresses, which serve as the buckling driving force, remain essentially the same in magnitude within such a thickness range.

The buckling problem for an actual panel in Fig. 2 is difficult to be analytically solved from Eq 1. Thus, a finite element-based buckling distortion analysis procedure was proposed below.

2.2 Finite Element-Based Buckling Distortion Analysis

The detailed weld residual stress analysis procedures will be discussed in this section, even though some of the procedures had been used in the past as discussed in some earlier publications (Ref 20-22). Typically, longitudinal (parallel to welding direction) tensile residual stresses occur in the weld and longitudinal residual compressive stresses occur in areas away from the weld in thin gauge plate components. If the compressive residual stress over a length scale that is comparable with buckling wave length exceeds the critical buckling load of weldment, buckling distortion will develop. With a full-field residual stress distribution, the "stress stiffening" matrix $[K]_{\lambda\sigma^r}$ can be formulated in the form that consistent with buckling stability analysis procedures within the context of finite element methods, such as:

$$\left([K]_t + \Delta\lambda_{cr}[K]_{\lambda\sigma^r}\right)\{u\} = \{0\} \qquad \text{(Eq 6)}$$

which can be solved for $\Delta\lambda_{cr}$ in a conventional manner under a given weld residual stress distribution. Note that $[K]_t$ is the conventional tangential stiffness matrix at a reference configuration, $\{u\}$ the corresponding displacement vector, typically referred as buckling mode shape.

Without considering weld residual stresses, Eq 6 typically provides multiple buckling mode shapes and the corresponding buckling loads (eigenvalues). With a full residual stress distribution being considered (as a pre-stress state), Eq 6 may miss the actual buckling mode by providing a higher order of mode, if the structure is already buckled due to the presence of a given residual stress distribution. In such situation, the residual stress field scaling parameter λ in Eq 1 or 6 will be progressively reduced until the lowest buckling mode is identified under given boundary conditions. In doing so, the present procedure provides an effective means in identifying the actual buckling mode without prior knowledge. If there are no additional modes being identified in this process, the lowest mode with $\lambda = 1$ is the most likely buckling mode.

For absolute magnitude distortion estimation in addition to shape, one additional step needs to be taken by including the identified buckling mode from Eq 6 to perform a nonlinear large deformation weld analysis. In the following, the above buckling analysis procedures are first demonstrated in a butt welded flat plate on which detailed experimental data are available.

3. Buckling Distortion Prediction

A full-penetration weld specimen and fixture are shown in Fig. 2. The specimen was made of low carbon steel with a length of 500 mm, width 200 mm, and thickness 2.5 mm. The weld was conducted with GTAW welding process with parameters: welding current 155 amps, welding voltage 13 V, and travel speed 5 mm/s. Both sides of the test specimens parallel to the weld line were clamped tightly by a hydraulic keyboard jig to ensure uniformity of pressure to simulate severe restraint conditions in production situations.

A 3-D shell element model of the specimen, as shown in Fig. 3, was adopted from an early study (Ref 22) where its application for modeling multi-pass welds was also presented.

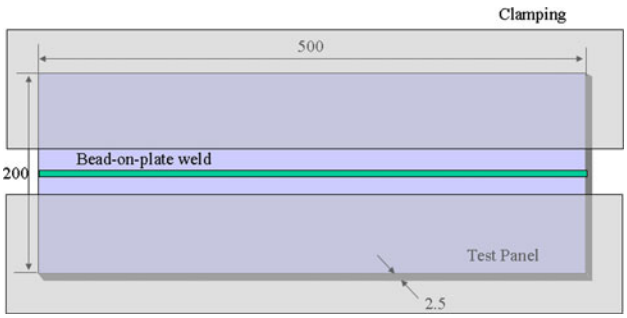

Fig. 2 Sketch of TIG welding of thin steel sheet

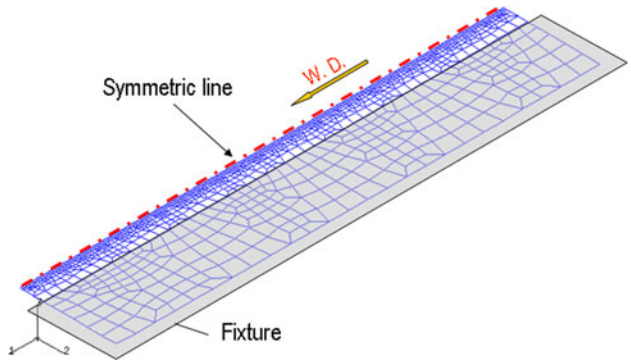

Fig. 3 Three-dimensional shell model

Very fine mesh was used in the weld and heat-affected zone to capture the localized stress distributions. Coarse mesh was used in the area away from the weld to reduce computational time. With the shell element model, the surface convection heat loss to the air from the top and bottom surfaces of the coupon sheet and the out-of-plane (in z-direction) deformation mode were considered. The thermal heat sink from the clamps was modeled by increasing heat convection coefficient in the clamping area. The through-thickness temperature and deformation gradients were resolved using five integration points along shell thickness directions based on an early study (Ref 22). Symmetry conditions were assumed with respect to the centerline of the weld. Fixed displacement boundary conditions (both in-plane and out-of-plane) were imposed at clamp positions (see Fig. 3) to simulate the clamping conditions during welding. The thermal physical properties (Ref 23) and mechanical properties are temperature-dependent that were input to the finite element models. The mechanical properties were obtained from materials testing at different temperatures.

3.1 Prediction by Conventional Thermoplasticity Analysis Procedures

To illustrate the requirements for buckling analysis procedure for unstable distortions, we start with a conventional residual stress and distortion analysis procedure without considering buckling. A moving heat source model was developed (Ref 20) and used as an ABAQUS user-subroutine in the form of surface heat flux. The top and bottom surfaces of the plate were subjected to convective heat loss at ambient temperature. The energy-density distribution of the moving arc was assumed to be of a Gaussian type. Figure 4 shows the temperature distribution on the test plate when arc was moving near the middle of the plate.

Using the temperature history from welding heat flow analysis discussed above, conventional residual stress/distortion analysis was performed. A weld material model was used in conjunction with ABAQUS, as discussed in Ref 5. By comparing the predicted final distortion shape with the experimental one in Fig. 5, it can be seen, as expected that the conventional thermoplasticity procedure cannot capture the buckling distortion behavior. However, this step is necessary in providing the full-field residual stress distribution that contributes to the stress-stiffening matrix in Eq 6.

3.2 Prediction by Present Buckling Analysis Procedure

By applying the buckling analysis procedure as embodied in Eq 6 with the full-field residual stress generated using the thermoplasticity analysis procedure, the buckling distortion analysis procedure was then performed after mapping the 3D full-field residual stresses on to the 3D buckling analysis model. It is critical to select the 3D full-field residual stresses after releasing the clamps. Residual stress strongly depends on the restraint conditions. Substantial clamping can, relative to minimal clamping, produce very different history effects on the overall outcome of residual stress and deformation following release. Note that the line force definition in Eq 1 should be applied to both longitudinal and transverse directions. Since a 3D shell element model was used in this investigation, the line force integration in through thickness direction is not needed if the stresses at the mid-section are used. Figure 6 shows that the welding residual stress has very strong effect on the eigenvalue of the buckling modes. For instance, the eigenvalues

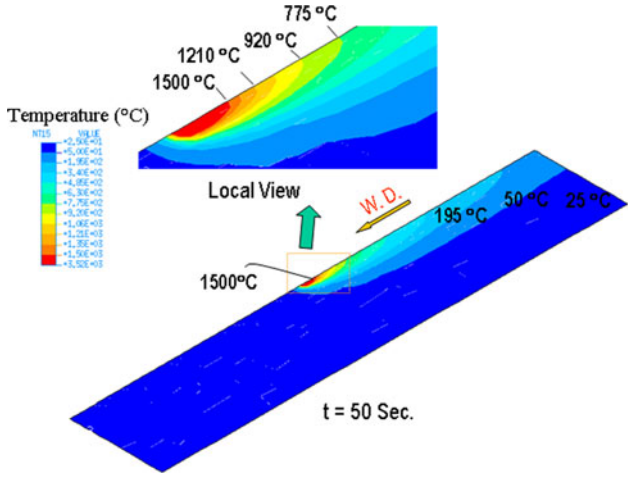

Fig. 4 Predicted temperature distribution of conventional welding on top surface

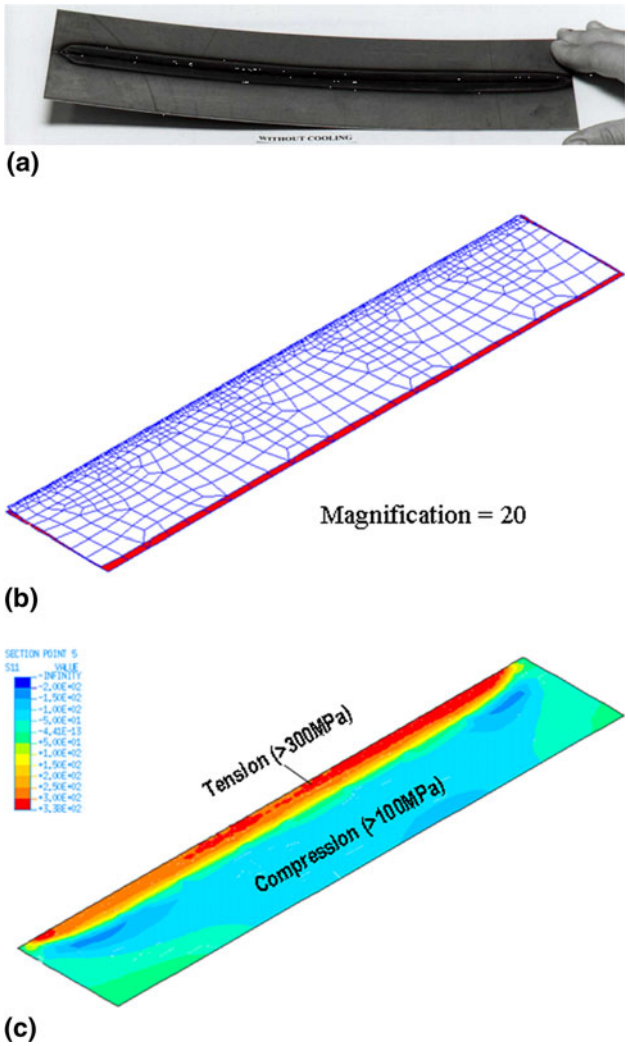

Fig. 5 Comparison between experiment and prediction without considering buckling. (a) Experimental distortion shape, (b) predicted distortion without considering buckling, and (c) weld residual stress

(or buckling strengths) for the first three modes were all significantly reduced, particularly for the first mode, which indicated a 45% reduction in the buckling strength under the given residual stress field predicted. If the specimen buckles, it must exhibit the buckling mode shape corresponding to the 1st mode. Thus, the first mode was chosen to include in the post-buckling analysis to establish both buckling shape and magnitude.

The major steps in the buckling analysis procedure can be summarized as follows: (1) perform conventional residual stress analysis, (2) identify the most likely buckling mode, and (3) conduct post buckling analysis. Using this procedure, the buckling distortion corresponding to the full-field residual stress distribution (Fig. 5c) was predicted, as shown in Fig. 7. The predicted buckling distortion is rather consistent with the experimental results (Fig. 5a) in both buckling shape and magnitude.

4. Buckling Distortion Mitigation Techniques

The discussions in the previous sections suggest that any effective buckling mitigation techniques must consider either (1) reducing buckling driving force (weld residual stress distribution and it magnitude in compression) or (2) increasing buckling resistance (thickness or aspect ratio, a/b), or both. In what follows, for the given butt-welded thin plate, some of the effective techniques in reducing buckling driving force will be demonstrated by considering two in-process mitigation techniques:

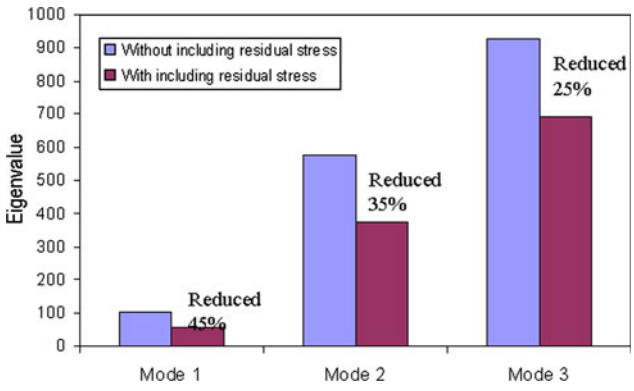

Fig. 6 Eigenvalues with and without including residual stress

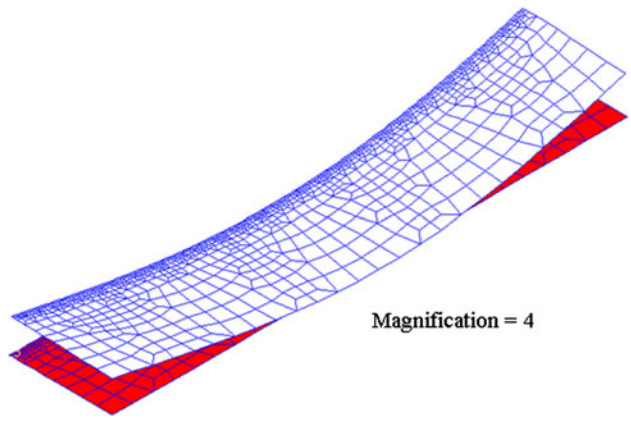

Fig. 7 Distortion predictions with considering buckling

4.1 Trailing Heat Sink Technique

The trailing heat sink technique is illustrated in Fig. 8. The test specimen shown in Fig. 2 was used for this study. Liquid nitrogen was selected as a cooling media. Cooling jet connected with a pressurized liquid nitrogen supply system (Ref 20) introduces a localized heat sink at a given distance behind the arc. The distance between the welding torch and the cooling nozzle remain constant during welding. The distance was selected by experiment and modeling for optimal performance. Experiments show that three technological parameters, the cooling distance, flowing rate of liquid nitrogen, and cooling width (diameter of cooling jet) determine the specific characteristics and the intensity of the heat sinking system. For a specified joint geometry, materials and welding heat input, the trailing heat sink parameters were investigated first using detailed finite element simulations to identify some of the important parameters and their approximate ranges. Then, the experimental studies were performed to validate and refine some of the process parameters.

The trailing heat sink technique was investigated with the finite element methods described in the previous sections. The same finite element model shown in Fig. 3 was used here. The trailing heat sink was modeled by introducing a user subroutine in ABAQUS (*FILM) to simulate the intense cooling effects due to the presence of a heat sink. After some preliminary analyses, the resulting energy density within the heat sink area was assumed to be uniform. Heat sink media was liquid nitrogen with heat of vaporization 160 J/cm^3 and boiling temperature −196 °C (Ref 24) and the applying radius of cooling source was assumed to be 5 mm in the thermal analysis.

Figure 9 shows an instantaneous temperature distribution when welding arc is moving to the middle of the plate with the trailing heat sink technique. Comparing with Fig. 4 (without trailing heat sink), a zone of temperature depression (low temperature zone) is clearly seen behind the arc in Fig. 9. This low temperature zone provides a stretching effect on the weld metal undergoing a rapid cooling so that the weld metal shrinkage can be reduced, resulting in not only significantly reduced final residual stresses, but also altered overall distribution (see Fig. 10b) compared with that without trailing heat sink in Fig. 5(c). For instance, the compressive longitudinal residual stresses are distributed over a long range with respect to the plate size in Fig. 5(c), while they become confined to a

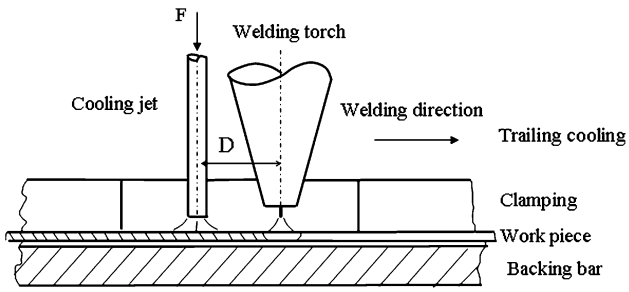

Fig. 8 Welding setup of trailing heat sink

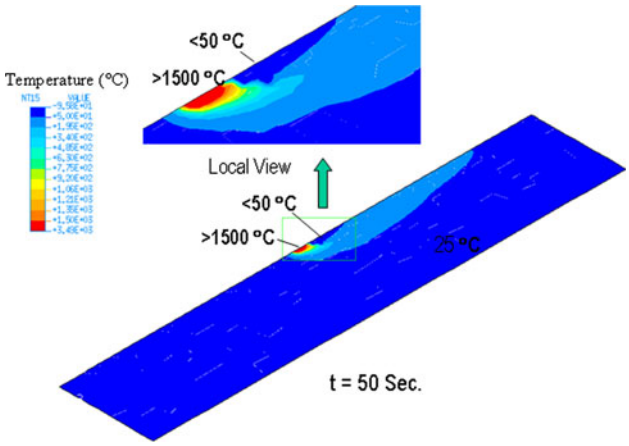

Fig. 9 Temperature distribution op top surface of welding with trailing heat sink

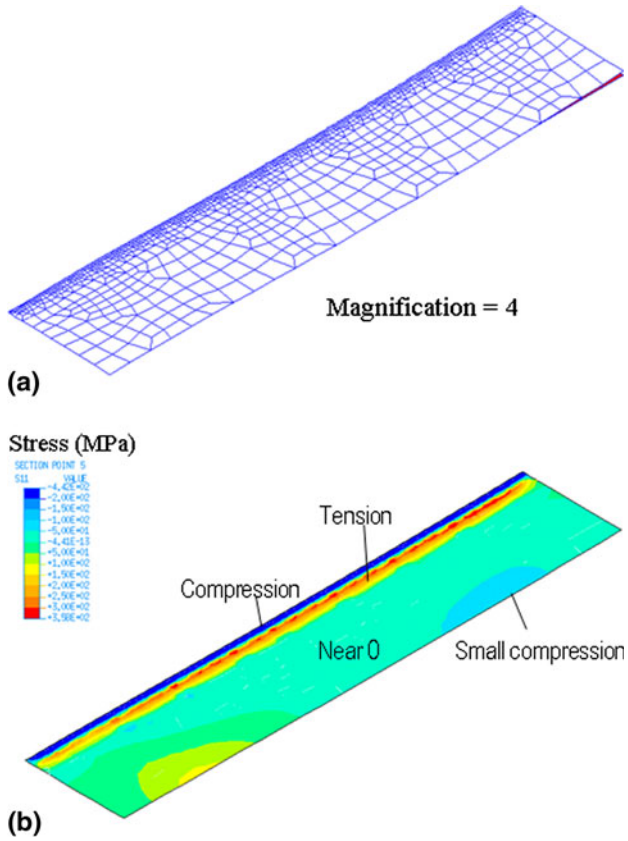

Fig. 10 Distortion and residual stress of welding with trailing heat sink. (a) Final distortion, (b) longitudinal residual stress

small area in Fig. 10(b). As a result, the buckling driving force can be reduced or eliminated. The predicted final distortion by using the 1st mode with nonlinear large deformation procedure is shown in Fig. 10(a). The final distortion was very small which proves the effectiveness of the trailing heat sink technique. Figure 11 shows the experimental validation of the trailing heat sink technique proposed. By welding with the trailing heat sink, welding buckling distortion was significantly reduced when compared to the conventional-welding-induced distortion shown in Fig. 5(a).

Fig. 11 Experimental validation of trailing heat sink technique

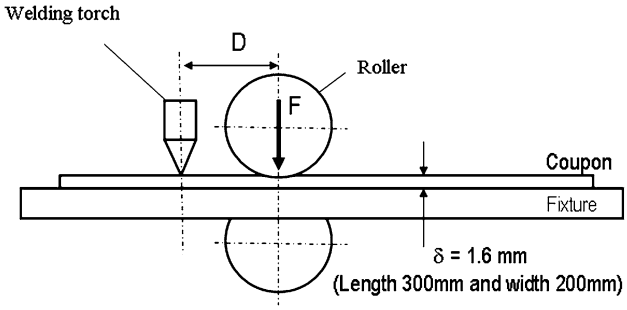

Fig. 12 In-process rolling welding setup. *F*, Rolling force, W_r, roller width (profiles), D, rolling distance

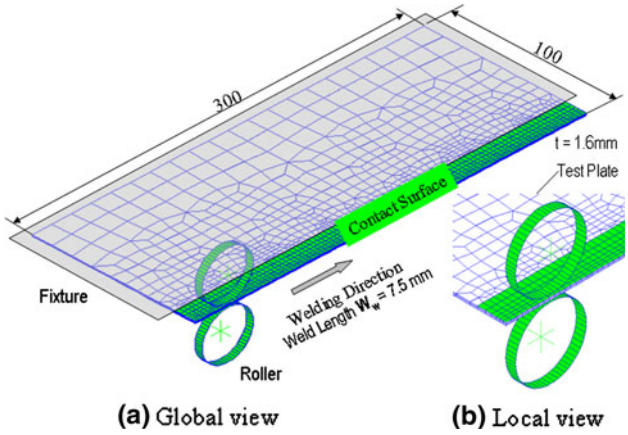

Fig. 13 Finite element model for in-process rolling. (a) Global view, (b) local view

4.2 In-Process Rolling Technique

The in-process rolling technique is illustrated in Fig. 12. During welding, both rollers can be placed opposite to each other against the specimen at a distance behind the traveling torch. By rolling the weld which is subjected to compressive plastic deformation in the through-thickness direction, the weld metal elongates in the welding directions, resulting in reduced residual stresses. Some of the major rolling parameters are rolling force, roller width, and the distance between the welding torch and the roller. It should be pointed out that it is not necessary to have both top roller and bottom roller. For instance, if a solid support can be used at the plate bottom, only the upper roller is needed.

A 3-D solid model with the contact considerations between the roller and the weldment was used to simulate this complicated process, as shown in Fig. 13. One half of the plate was modeled by considering the structural symmetry with respect to the weld centerline, as shown in Fig. 13, in which the two rollers were simulated as rigid bodies. The specimens to be

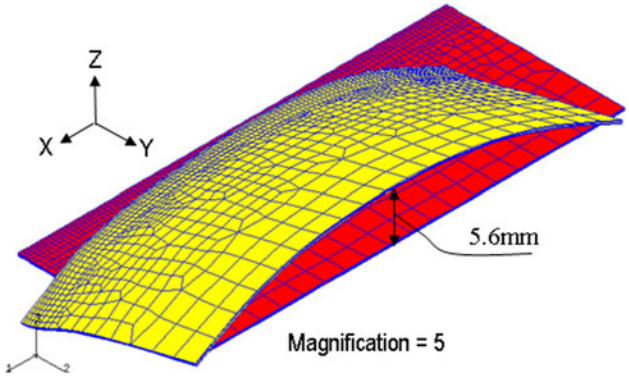

Fig. 14 Welding distortion with conventional welding

welded were made of high strength Al-Li alloy with 200 mm width and 300 mm length. The thermal-physical and mechanical properties at room temperature can be found in Ref 4.

The transient 3D welding heat flow analysis procedure with a moving arc follows the same procedure as discussed earlier. The thermomechanical analysis following the temperature history requires modeling the contact interactions between the weldment and the rollers, as shown in Fig. 13. As a result, the solution process is often slow. With this model, various rolling parameters such as, the roller force (F), the roller width (W_r), and the rolling distance (D) can be investigated to establish their effects on residual stress reductions.

For comparison purposes, conventional welding without in-process rolling was simulated and the predicted buckling distortion is shown in Fig. 14 using the analysis procedures discussed in the earlier sections. A deflection of 5.6 mm in Z direction in the middle of the plate length was predicted. The results corresponding to two levels of roller force are summarized in Fig. 15. Figure 15(a) shows the temperature distribution at one moment in time and the corresponding process parameters. Note that one half roller width (W_r) is used in the model due to symmetry. Both the roller width and the rolling distance (D) were kept constant in Fig. 15. When F = 4.2 kN was applied during welding, the predicted buckling distortion was reduced, as shown in Fig. 15(b), comparing with that without in-process rolling shown in Fig. 14. By conducting several numerical experiments, it was found that F = 5.5 kN is the minimum rolling force to completely eliminate the buckling distortion, as shown in Fig. 15(c). This is because the rolling action produces sufficient in-plane stretching effect on the material away from the weld. This stretching effect reduces the tensile stresses in the weld area and almost eliminated the compressive residual stresses next to the weld, as shown in Fig. 16. Consequently, buckling driving force is reduced.

The roller width also has a strong effect on the weld buckling distortion. In addition to its obvious effects on the average contact pressure, a proper roller width should be measured with respect to the width of the weld due to the fact that nonlinear contact interactions are confined within the weld metal experiencing a relative high temperature. For instance, it was found that if the roller width was increased 1.5 to 2.3W_{eld}, and the rolling force needs to be increased from 5.5 to 6.8 kN to be effective.

The roller to torch distance is another critical parameter for the in-process rolling technique. With the rolling distance increasing, the weld metal temperature becomes lower, and

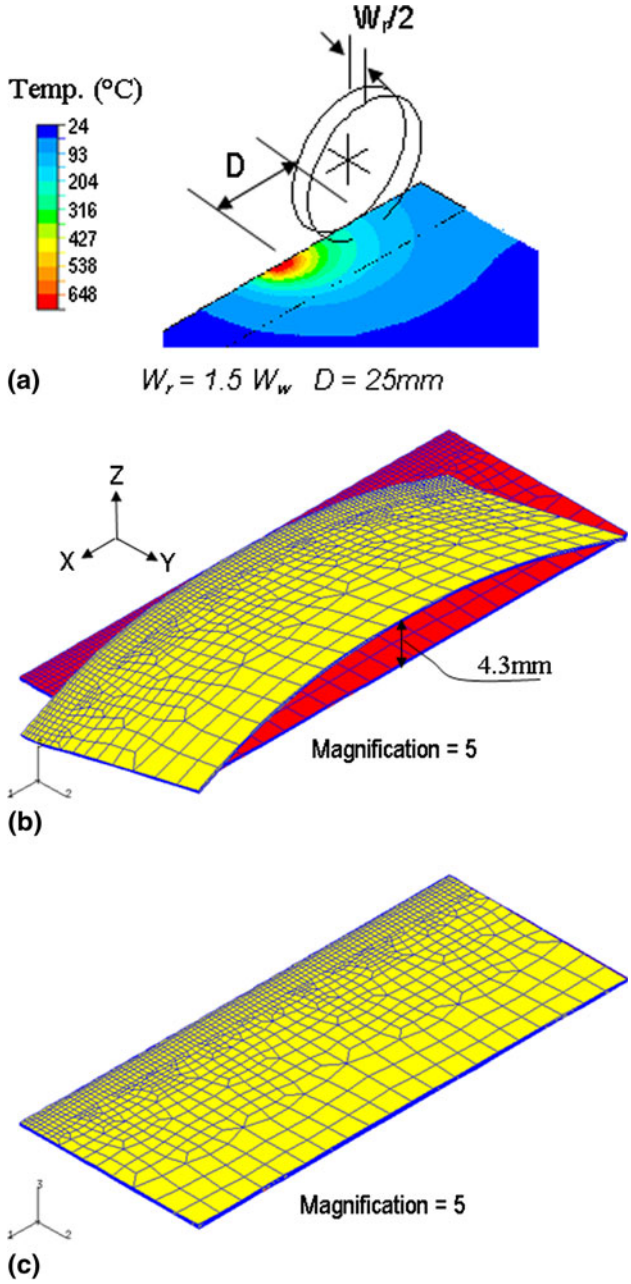

Fig. 15 Effect of rolling force (F) on welding distortion. (a) Temperature distribution, (b) in-process rolling (F = 4.2 kN), and (c) in-process rolling (F = 5.5 kN)

hence a higher rolling force is needed to achieving the same stretching effects. If the rolling distance is increased to 45 mm, the rolling force has to be increased to 7.8 kN to eliminate the buckling distortion. These results suggest that the three rolling parameters can be related to each other for optimum effectiveness for a particular application.

5. Summary

In this article, the buckling distortion mechanisms in thin section structures have been discussed in detail by means of both the classical buckling theory and the finite element

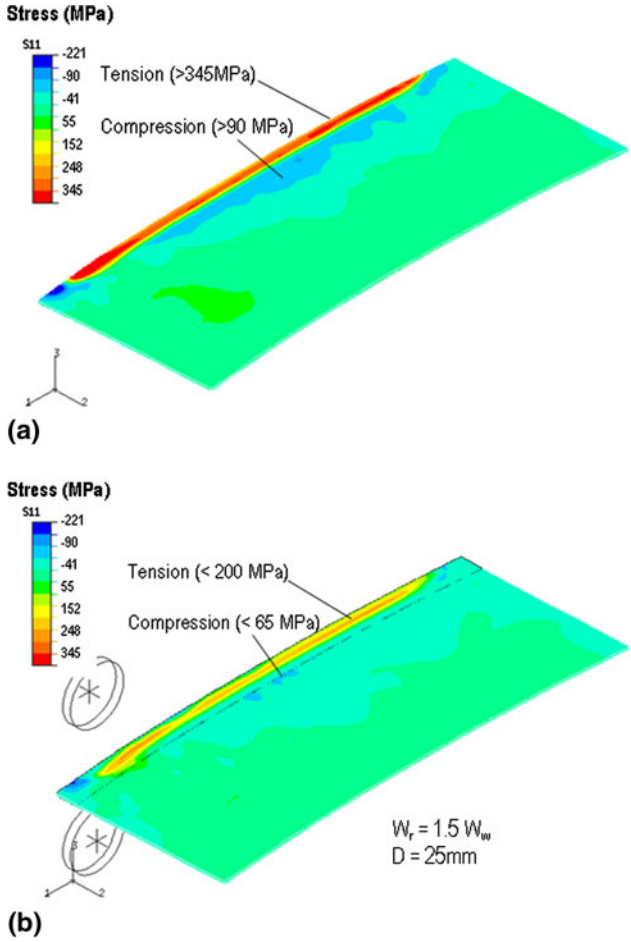

Fig. 16 Effect of rolling pressure (F) on longitudinal residual stress. (a) Conventional welding, (b) in-process rolling (F = 5.5 kN)

procedures. With the classical buckling theory, some of the important parameters controlling buckling resistance of a given structure are discussed. With the detailed finite element procedures presented, the buckling driving force in terms of both residual stress magnitude and its distribution are quantified. It has been demonstrated that to effectively mitigate buckling distortions, one can either maximize the buckling resistance (such as plate aspect ratio a/b) and/or minimize the buckling driving force, which can be altered by reducing welding-induced residual stress magnitude and/or distributions. Along this line, two effective buckling distortion mitigation techniques have been demonstrated by both reducing residual stress magnitude and achieving a favorable distribution: (1) trailing heat sink technique; and (2) in-process rolling technique, both of which were validated by experimental results. Their underlying principles are also illustrated with detailed finite element results.

References

1. K. Masubuchi, Research Activities Examine Residual Stress and Distortion in Welded Structures, *Weld. J.*, 1991, **70**(12), p 41–47
2. A.K. Dhingral and C.L. Murphy, Numerical Simulation of Welding-Induced Distortion in Thin-Walled Structures, *Sci. Technol. Weld. Join.*, 2005, **10**(5), p 528–536
3. Y. Ueda, K. Nakacho, and T. Shimizu, Improvement of Residual Stresses of Circumferential Joint of Pipe by Heat-Sink Welding, *J. Press. Vessel Technol.*, 1986, **108**, p 14–23
4. P. Dong, J.K. Hong, and P. Rogers, Analysis of Residual Stresses in Al-Li Alloy Repair Welds and Mitigation Techniques, *Weld. J.*, 1998, **77**(11), p 439s–445s
5. P. Dong, Residual Stresses and Distortions in Welded Structures: What We Know Today and Beyond, Keynote Lecture, *Proceedings of 6th International Conference on Trends in Welding Research.* S.A. David, T. DebRoy, J.C. Lippold, H.B. Smartt, and J.M Vitek, Ed., ASM International, 2002, p 815–825
6. Y.P. Yang, P. Dong, F.W. Brust, J. Zhang, and Z. Cao, Numerical Prediction of Welding-Induced Buckling Distortion and Buckling Mechanisms, *Adv. Comput. Eng. Sci.*, 2000, **2**, p 1906–1912
7. Y. Yang, R. Dull, C. Conrardy, N. Porter, P. Dong, and T.D. Huang, Transient Thermal Tensioning and Numerical Modeling of Thin Steel Ship Panel Structures, *J. Ship Prod.*, 2008, **24**(1), p 37–49
8. M.V. Deo, P. Michaleris, and J. Sun, Prediction of Buckling Distortions of Welded Structures, *Sci. Technol. Weld. Join.*, 2003, **8**(1), p 55–61
9. P. Michaleris and X. Sun, Finite Element Analysis of Thermal Tensioning Techniques Mitigating Weld Buckling Distortion, *Weld. J.*, 1997, **76**(11), p 451s–457s
10. M.V. Deo and P. Michaleris, Mitigation of Welding Induced Buckling Distortion Using Transient Thermal Tensioning, *Sci. Technol. Weld. Join.*, 2003, **8**(1), p 49–54
11. E.M. Van der Aa, M.J.M. Hermans, and I.M. Richardson, Conceptual Model for Stress and Strain Development During Welding With Trailing Heat Sink, *Sci. Technol. Weld. Join.*, 2006, **11**(4), p 488–495
12. J. Li, Q. Guan, Y.W. Shi, and D.L. Guo, Stress and Distortion Mitigation Technique for Welding Titanium Alloy Thin Sheet, *Sci. Technol. Weld. Join.*, 2004, **9**(5), p 451–458
13. D.G. Richards, P.B. Prangnell, P.J. Withersl, S.W. Williams, T. Nagy, and S. Morgan, Efficacy of Active Cooling for Controlling Residual Stresses in Friction Stir Welds, *Sci. Technol. Weld. Join.*, 2010, **15**(2), p 156–165
14. Q. Guan, C.X. Zhang, and D.L. Guo, Dynamic Control of Welding Distortion by Moving Spot Heat Sink, *Weld. World*, 1994, **33**(4), p 308–312
15. Y.I. Bural, Y.P. Romanchuk, A.A. Kazimirov, and V.P. Morgun, Selection of the Optimum Fields for preheating Plates Before Welding, *Avt. Svarka*, 1979, **5**, p 5–9
16. Y.P. Yang, P. Dong, X. Tian, and J. Zhang: Prevention of Welding Hot Cracking of High Strength Aluminum Alloy by Mechanical Rolling, *Proceeding of 5th International Conference on Trends in Welding Research*. S.A. David, J.A. Johnson, H.B. Smartt, T. Debroy, J.M. Vitek, Eds., ASM International and American Welding Society, 1998, p 700-709
17. J. Altenkirch, A. Steuwer, P.J. Withers, S.W. Williams, M. Poad, and S.W. Wen, Residual Stress Engineering in Friction Stir Welds by Roller Tensioning, *Sci. Technol. Weld. Join.*, 2009, **14**(2), p 185–192
18. D. Xu, X.S. Liu, P. Wang, J.G. Yang, and H.Y. Fang, New Technique to Control Welding Buckling Distortion and Residual Stress With Noncontact Electromagnetic Impact, *Sci. Technol. Weld. Join.*, 2009, **14**(8), p 753–759
19. S.T. Timoshenko, *Theory of Elastic Stability*, 2nd ed., McGraw-Hill, New York, 1961
20. Y.P. Yang, P. Dong, J. Zhang, and X. Tian, A Hot-Cracking Mitigation Technique for Welding High Strength Aluminum Alloy Sheets, *Weld. J.*, 2000, **79**(1), p 9s–17s
21. Y.P. Yang, F.W. Brust, Z. Cao, J. Zhang, J.K. Hong, A. Fisher, R. Broman, and R. Thakkar, Modeling Tool Development of Weld Process for Thin Plate Automotive Application. *International Conference on Computer Engineering and Science*. S.N. Atluri and F.W. Brust, Eds., Tech Science Press, 2000, p 1989-1905
22. J. Zhang, P. Dong, F.W. Brust, Composite Shell Element Model for Residual Stress analysis of Multi-Pass Welds. *Transaction of the 14th international Conference on Structural Mechanics in Reactor Technology*, Vol 1, M. Livolant Ed., The International Association for Structural Mechanics in Reactor Technology, 1997, p 335–344
23. ASM International, *Metals Handbook*, 1990, **1**, p 195–197
24. A.G. Rose-Innes, *Low Temperature Technique*, Vol 140, D. Van Nostrand Company, Inc, Princeton, 1965